A Lab-on-a-Chip Design for Cancer-Associated-Fibroblast Transcriptomic Profiling

Emily Gu, Jasmine Gupta, Joshua Lin, Arjit Misra, Eliott Park

***Abstract*—Recent research has indicated that interactions between cancer cells and the stroma may play a pivotal role in the onset of metastasis–the primary cause of cancer death. Studies have gradually clarified the role of cues from tumor microenvironments through cancer-on-a-chip models, which utilize microfluidic chips with small chambers for cell culturing along with other controllable parameters. Specifically, carcinoma-associated fibroblasts (CAFs) have been determined to play major roles in the progression of cancer. We present a co-culture device that will examine CAF recruitment at single-cell resolution by means of single cell RNA sequencing (scRNA-seq). This device includes a primary and secondary chip and operates through two cycles: recruitment and flush. The primary chip has three overlaid layers that include the co-culture chambers, a pneumatic valve system, and exit channels. The second chip consists of microfluidic channels designed for generating single cell droplets to be used by sequencing analyzers. Co-culturing in parallel wells allows for paracrine signaling, which leads to the recruitment of fibroblast candidates by the tumor cell lines. The migration of fibroblasts will be detected using real time imaging, and valves will control the exit channels. Media is delivered in two parallel channels lying perpendicular to the migration channels. We believe our device can be utilized to benefit future cancer research endeavors. We did not test our device due to the scope of our project, and we acknowledge that there are potential ideas/issues that could be further addressed.**

I. Introduction

For years, researchers have tried to dissect the stages of carcinogenesis, focusing primarily on direct alterations to cancer cells genetically and epigenetically. However, current studies in genetics and cell biology have indicated that tumor growth is not only determined by the malignant founder cells, but also the surrounding tumor stroma. [**?**]. The harmful effects of cancer cells cannot be manifested without interaction between cancer cells and their local environment. A typical tumor structure consists of cancer cells and other surrounding stromal cells in the tumor microenvironment, such as fibroblasts, lymphatic endothelial cells, immune cells, and angiogenic vascular cells. Fibroblasts are one of the largest components of the stroma. CAFs can be defined as a cell type that promotes tumorigenic features by secreting cytokines.[**?**] Investigation of the critical molecular factors that contribute to tumor evolution is important as these serve as potential targets for therapeutic development.[**?**] Thus, our group decided to synthesize a device specific to this topic.

CAFs are hypothesized to influence tumor progression through cell–cell interactions and secretion of extracellular matrix components (ECM), chemokines, and more. Furthermore, CAFs are commonly found next to cancer cells, and can be identified by their expression of α-smooth muscle actin (α-SMA). Traditional *in vitro* studies of tumor cell processes have been conducted with commercially available transwell chambers by measuring the density of cells migrating vertically through a gel into a filter. However, many specific details still remain unclear. Recent studies have looked at utilizing microfluidic 3D environments for cell co-culturing, however these existing systems are limited to co-culturing on 2D surfaces at initial stages. Additionally, cells are usually engulfed by ECM in *in vivo* environments, and syringe pumps are used to pattern cells in the 3D matrix. Unfortunately, complicated protocol for existing systems limit their real biological and research applications. [**?**] In this paper, we present a microfluidic-based co-culture device that will examine CAF recruitment at a single-cell resolution using scRNA-seq. In theory, the tumor cells and fibroblasts will be co-cultured during the whole experimental period. This is a suitable platform for investigating mechanisms of CAF recruitment in a well defined cellular environment.

II. Device overview

Chip 1

The overall operation of the device comprises two distinct cycles:

- **The recruitment cycle:** Organotypic co-culture in the parallel wells enables cell-cell communication via paracrine signaling, and will cause recruitment of fibroblast candidates (and induction of CAFs) by the tumor cell lines.
- **The flush cycle:** When cellular migration is detected by a real-time imaging camera, that specific migration channel is flushed such that the migrated cells are translocated to the exit channels, which span the middle and base layer. The exit channel is flushed via the flush channel and cells are thus sent to collection chambers.

Media is delivered through two parallel channels orthogonal to migration channels. The flow rates are matched during the recruitment cycle, such that the fluid media in the migration channels is static and delivery of nutrients is diffusion-based only. This is further elucidated in the Media Delivery subsection. branching out from each migration channel is an exit channel, which is sealed during the recruitment cycle.

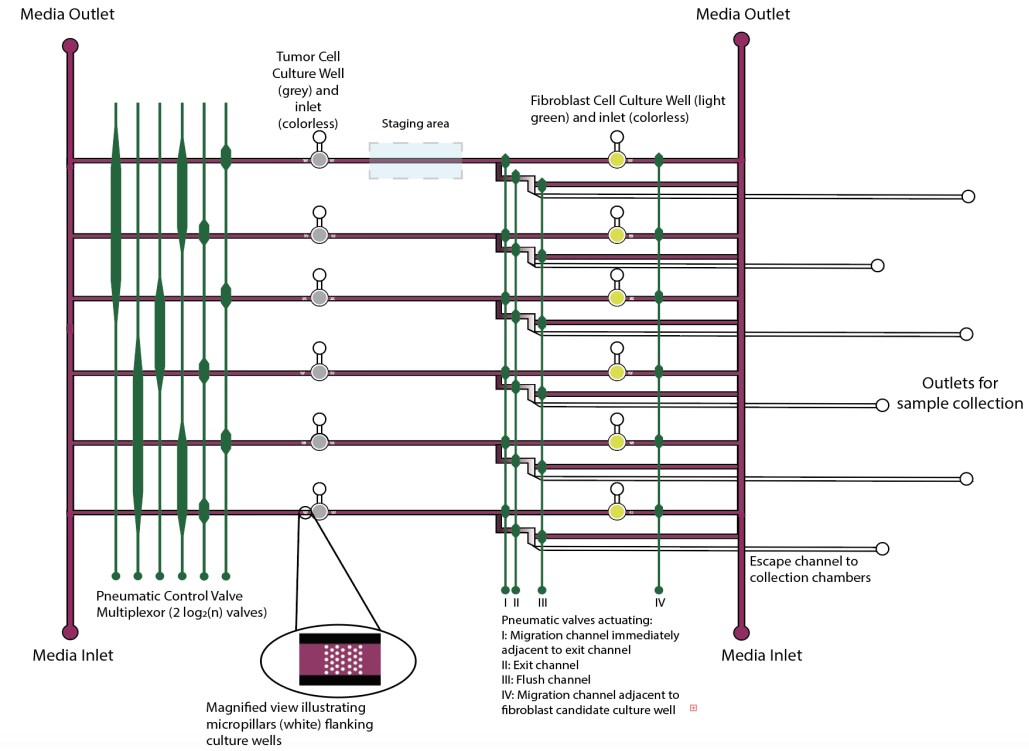

Fig. 1. Overview schematic of complete chip 1. All pneuamtic control valves are in green, and are situated on layer 4. Migration, flush, and exit channel beginnings (red) are on layer 2, and collection channels and chambers (colorless) are on layer 1 (base layer).

Chip Layout

The first chip is made up of four distinct layers. As shown in Figure 1, the four layers will be overlaid to form the complete chip. The bottom most layer contains the outlet channel and well for sample collection after they are flushed out of the migration channel. This layer also extends out farther than the middle and top layers, allowing researchers access to the collection wells for sample transport. The topmost layer contains the actuation channels for the valves. The 3rd layer contains the co-culturing system and migration channel. The second layer contains only micropillars extending into the migration channels. Bordering either side of the middle layer are the media supply channels. Running perpendicular to the test channels, they are 800μm wide and 50μm deep. The length of the channel depends on the number of samples being tested, each test sample spanning around 1.5mm with space on either side. The cross channels connecting the two media channels do not have media flowing through them but instead rely on diffusion for nutrients. They are 6840umX300μmX50μm. The tumor cell culture well is a 1mm diameter circle with a depth of 50μm. The fibroblast culture chambers are 320μm in diameter and 50um deep.[**?**]

Media Delivery

As observing CAF migration may take days, we must constantly deliver the proper nutrients in order for the samples to survive. For our proof of concept and because there was sufficient literature regarding tumor consumption rate, we used oxygen as the nutrient on which we conditioned the length of the channel between the media delivery channel and the chambers.[**?**] This system can be extended to include multiple nutrients, in which case the concentrations and consumption rates of each would have to all equalize over the same distance. As mentioned above, the channel depth $Z = 50\mu$m, and the flow rate of the media Q_o = 5.8094*10^{-}11m^3/s. We found the diffusion constant of oxygen in media to be $D_o = 3.00 \times 10^{-5}\,\mathrm{cm}^2/\mathrm{s}$ and the tumor consumption rate of oxygen to be $R_o = 3.53 \times 10^{-4}\,\mathrm{mol}/\mathrm{cm}^3$ for a tumor with a 500 micron diameter. [**?**] [**?**] We may choose our own media concentration to condition the distance between the chamber and the media channel, L. The only constraint we have is that L must be greater than or equal to the width of the pneumatic valve system and the width of the micropillar array, which we will call W_m and is equal to 100um. Our valve channel width, W_v, comes out to be 200 microns and our resolution r is 10 microns. The overall width of all valve channels scales with the number of valves, N_v. The number of migration channels, and thus the number of cell populations we are studying, which we will call N_c, determines the number of valves due to the scaling of the multiplexor. [**?**]:

$$N_v = 2log_2(N_c) \tag{1}$$

The relationship between cell populations and L is defined below:

$$L = (W_v + r)N_v + W_v \tag{2}$$

For the current iteration of our device, we use 6 cell populations. Plugging in correspondingly yields a minimum length including the micropillar array L = 2620μm.
We calculate the relationship between length and cell media oxygen concentration C_o by setting the rate at which oxygen enters the tumor chamber, A_o, equal to the oxygen consumption rate of the tumor, R_o, as seen in Fig. 2.

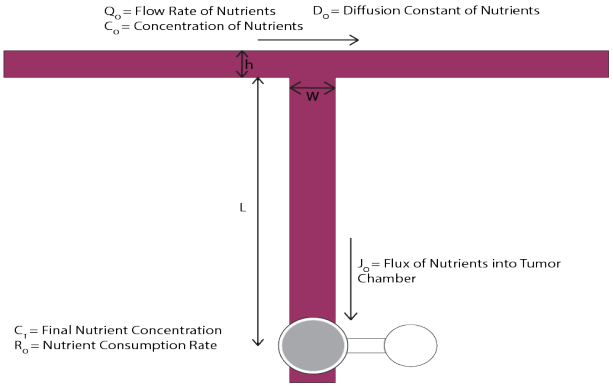

Fig. 2. Zoomed in view of media channel with oxygen diffusing to tumor chamber.

We solve for A_o with the diffusive flux J_o of oxygen entering the tumor chamber:

$$A_o = |J_o|WZ \tag{3}$$

J_o can be found with the concentration gradient in the channel, C_b, using Fick's first law:

$$|J_o| = D_o|\frac{dC_b}{dy}| \tag{4}$$

Since the oxygen concentration in the media channel is always constant and the concentration at the chamber will be consumed (equal to 0), we know that C_b is linear and thus can solve for it linearly:

$$|J_o| = D_o\frac{C_o - C_T}{L}$$
$$|J_o| = \frac{D_oC_o}{L}$$

We set A_o equal to R_o as mentioned earlier and plug in J_o and solve for L in terms of C_o:

$$R_o = A_o$$
$$R_o = \frac{D_oC_o}{L}WZ$$
$$L = \frac{D_oWZ}{R_o}C_o$$

Plugging in our values yields the relationship:

$$L = 1.27 \times 10^{-5}\,\mathrm{cm}^4/\mathrm{mol}C_o \tag{5}$$

If we plug in the minimum required distance between the media channel and the chamber we yield:

$$C_o = \frac{2.62cm}{1.27 \times 10^{-5}\,\mathrm{cm}^4/\mathrm{mol}}$$
$$C_o = 2.06 \times 10^5\,\mathrm{mol/cm}^3$$

The required oxygen concentration in the media channel is $2.06 \times 10^5\,\mathrm{mol/cm}^3$ for a length between the media channel and the tumor culture chamber of 2620 microns. We were unable to find a consistent value for CAF oxygen consumption, so we will assume similar consumption rates of the CAFs and tumor cells. We impose the same distance between the media supply channel and the CAF chamber in order to allow us to use the same media supply and maintain oxygen delivery-consumption equilibrium.

As an array of factors contribute to CAF migration, we look to previous literature to predict the distance at which CAFs are recruited by tumors. Karamichos et. al. finds that the distance comes out to be 500 microns, which is the distance we will use between the tumor cell culture well and the fibroblast culture well [**?**].

Micropillars

We incorporated micropillars to prevent the fibroblasts/tumor cells from escaping and traveling to other portions of the device that they are not supposed to be in. We considered that the size and density of the micropillars may determine how this could be achieved. Our micropillars have micro-gaps of 8 microns, which is less than the diameter of cells that will be utilized. This value was determined according to existing literature, which also detail the fabrication of microfluidic co-culture devices [**?**]. Micropillars span for 100 microns of our microchannel. The dimensions of the micropillars were optimized with the channel height. The height for our micropillars is 50 microns, and the diameter is 50 microns.
To account for the nature of PDMS, we checked our values from the displacement obtained from forces applied according to existing literature. The distributed force was represented by an equivalent point load on the micropillar, resulting in a deflection of the micropillar tip. Because our aspect ratio is less than 5 (value predetermined by literature), both bending and shear were taken into account in the force-deflection model (equation in literature). In all, the maximum displacement of the micropillar was calculated according to the equations. Force was calculated to be 1.125×10^{-10} N. This helped us determine the dimensions of our micropillars [**?**].
Additionally, we looked at how the micropillars affected the volumetric flow rate of liquid in the microchannel. The flow rate is defined as Q = dV /dt with V representing the volume of fluid inside the microchannel. According to literature, a derived flow rate ratio was determined where Q is flow rate in a cavity with pillars and Q[0] is flow rate in an empty cavity used for comparison [**?**].
The literature showcases the flow rate ratio Q/Q[0] as a function of the micropillar density φ and the micropillar aspect ratio h. Regardless of what the ratio h/d actually is, if the pillar density is small, Q/Q[0] tends to approach one. On the other hand when the pillar density is large, the ratio Q/Q[0] approaches zero. It is noticed that the higher the density of micropillars, the slower the flow rate Q in a control cavity with pillars, compared to the case of an empty cavity. Therefore, it can be concluded that the addition of micropillars does not enhance the pumping properties of a microchannel [**?**].

Priming

To seed the cells in the chip, simply inject the proper amount of cells in the their respective inlets. Using data from previous fibroblast culturing procedures and and fitting a quadratic curve, the following equation can be found with x corresponding to the volume of media and y10^5 the number of cells.[**?**]

$$y = -0.002715x^2 + 0.623961x - 0.486748 \quad (6)$$

In addition to priming cells, we prime the exit chambers with cell media culture. We close off all migration channels on both sides (all multiplexor valves and valve IV in Fig. 1) to ensure that the primed cells are not exposed to the full force of the media inlet initially. The exit channel to the migration chamber (valve II in Fig. 1) is also closed off for the same reason. The valve between the right hand media channel and the flushing channel (valve III in Fig. 2) is opened to allow media to flow through the exit channels to the bottom layer and out to 2 ml centrifugation tubes where the CAF samples will be collected sent to the droplet generation chip. In this step, just enough media is pumped through to allow for the connection tube outlet to be submerged in fluid inside of the centrifugation tubes. This allows us to assume atmospheric pressure as the final pressure at the end of the escape channels.

Flushing Cells

As previously discussed, the migration of fibroblasts will be detected using real time imaging. Once the fibroblasts have traveled past the exit channel, a series of valves will open or close to facilitate flushing. The valves directly on either side of the fibroblast culture chamber will close stopping any migrated fibroblasts from returning to the chamber. The exit channel valve and corresponding valve in the multiplexor are opened allowing migrated fibroblasts to be flushed into the exit valve using the left media channel. Then the flush channel valve below the migration channel gets opened allowing use of the right media channel to help move the cells from the entrance of the exit channel, leaving the chip and arriving at the external collection chambers.

While flushing the cells, we want to ensure that we do not apply excess stress that could affect the morphology or lyse the cells. Thus we calculated the max velocity and therefore max volumetric flow rate that the flushing can reach. Using the following work balance, one can solve for velocity. Inputting the critical shear stress for lysis of 0.75 Pa and the channel dimentions will give the maximum velocity of 0.03872 m/s.[**?**] This calculation also assumes the mass of the cells and media are similar to the mass of water.

$$Fl = \frac{mv^2}{2}$$

$$v = \sqrt{\frac{2PAl}{m}} \quad (7)$$

From the max velocity, we can also calculate the maximum volumetric flow rate as shown in equation 7. Thus the maximum volumetric flow rate = 5.8094*10^{-}10m^3/s to ensure that the cells do not lyse. As an additional engineering safety factor, the flow rate during flushing will not exceed 1/10 of this maximum flow rate.

$$Q = \frac{V}{t} = \frac{Ax}{t} = Av \quad (8)$$

Pneumatic Control

To actuate our device, we propose push-down pneumatic valves. All valves are fabricated on the topmost layer, layer 3. Longitudinal sections along the media channel and an actuation channel are shown:

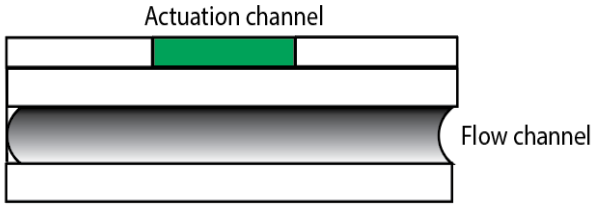

Fig. 3. Longitudinal section along the media channel

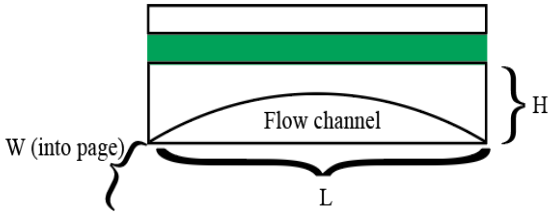

Fig. 4. Longitudinal section along the actuation channel. Note the parabolic arch of the flow channel.

We define the maximal height of the flow as d, the minimum thickness of the bottom half of the slab $H/2 - d = h$ and the pressure in the valve as P. Kartalov et. al show that a pneumatic valve may be modeled as a superposition of three basic mechanical models: a thick beam, thick spring, and thin spring[**?**]. They further report the Young's modulus of elasticity for PDMS to be 0.36 MPa. We will follow their work to derive actuation pressures for our device operations. We will not deviate from their evaluation of thin and thick spring models. (The thin spring model assumes the membrane is equivalent to a thin spring that contracts as the valve closes; the thick spring model assumes the membrane is equivalent to a suspension bridge across the flow channel, supported by two beams.) However, for the first (thick beam) model, Kartalov et. al modeled the valve as a series of two thick beams with uniform rectangular cross-sections. Here, we will use a single thick beam with non-uniform cross section along the length L of the valve, such that the lower bound of the beam is given by a parabolic arc, $-ax^2 - h$, where

$$a = \left(\frac{H}{2} - h\right)\frac{4}{L^2}. \quad (9)$$

The moment of inertia, I is given by

$$I = \iint_A y^2 dA$$

$$I = \int_{-\frac{W}{2}}^{\frac{W}{2}} \int_{-ax^2-h}^{\frac{H}{2}} y^2 dy dx$$

Then, upon integration, we obtain:

$$I = \frac{5a^3W^7 + 84a^2W^5H + 560aW^3H^2 + 280W(8H^3 + d^3)}{6270} \tag{10}$$

The deflection of a thick beam is given by:

$$\begin{aligned} & \delta = FL^3/3EI \\ \text{here,} \quad & \delta = d \\ & F = PWL \\ & P = \frac{3dEI}{WL^4} \end{aligned}$$

Combining all our thick beam model and the thin and thick spring models from Kartalov et al, and accounting for true strain, we arrive at the following final model, where I is as derived previously:

$$P = E \cdot ln\Big(1 + \frac{3dEI}{WL^4} + 16\frac{d^2}{3}\Big(\frac{1}{W^2} + \frac{1}{L^2}\Big) + 64\Big(\Big(\frac{1}{W^4} + \frac{1}{L^4}\Big)\Big(\frac{d^3H}{3} - \frac{d^4}{5}\Big)\Big)\Big)$$

Based on literature, we know that actuation pressures of 200kPa are relatively easily accessible [**?**]. We modeled the pressures necessary to actuate the flow channels given our migration channel dimensions (300 µm wide and 50 µm high) and height of the slab 100 µm. We arrive at the following dimensions:

- Actuation channel width over regions of actuation = 200 µm, required pressure = 182kPa.
- Actuation channel width over regions that must not be actuated = 200 µm, required pressure = 13.6MPa.

Thus, we will use maximal pressures of about 200kPa for channel actuation, which will tightly seal regions of actuation but will not affect orthogonal channels where actuation channel width is narrow.

CHIP 2

The second device combines existing methods for droplet generation and serves as a potential intermediary circuit between the culturing and recruitment device and the ensuing sequencing phase. Much simpler in design compared to chip 1, the device consists of five inlets for the dispersed phase (CAFs, barcoded beads, and PCR reagents) and continuous phase (oil), two junctions (coflow droplet generation and micropillar merger), and an exit channel. Here, we briefly outline the rudimentary workings for our secondary chip, which is based on the Ab-seq workflow as described by Shahi et al. As CAFs are not identical, this gives us insight as to the individual protein make up of these CAFs and will hopefully allow us to recognize patterns as to which particular protein markers determine cell recruitment. Further reading for an advanced technical overview is recommended.

Droplet generation

After exiting the first device, sorted single-cell CAFs enter an inlet flow channel where they are joined with gel barcoded beads at a Y junction and enter a flow-focusing droplet generator. Devices parameters such as channel geometries, viscosities of the two phases, and flow pressure are controlled such that the barcoded beads with lysis buffer enter the junction at a much higher frequency compared to the CAFs to avoid double encapsulation. Then, CAF droplets and PCR reagents enter the following junction in an alternating order by synchronizing flow rates, and adjacent droplets are merged two to one as they pass through the merging chamber. The resulting droplets exit the device ready for library preparation and sequencing.

scRNA-seq (transcriptomic profiling)

Following generation, the droplets are thermocycled, breaking the emulsion to allow DNA purification for library preparation. Then, the library is sequenced using an Illumina MiSeq kit following standard MiSeq sequencing protocol. To remove potential PCR and sequencing errors, we employ bioinformatic methods outlined by Shahi et al., which utilizes methods such as running raw barcode sequence reads through quality filters, selective data processing with group mapping, and UMI correction.

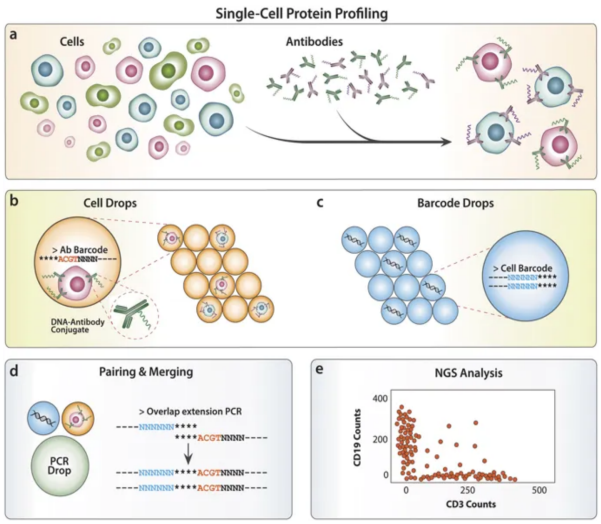

Fig. 5. Abseq workflow overview (Shahi, P., Kim, S., Haliburton, J. et al. 2017)

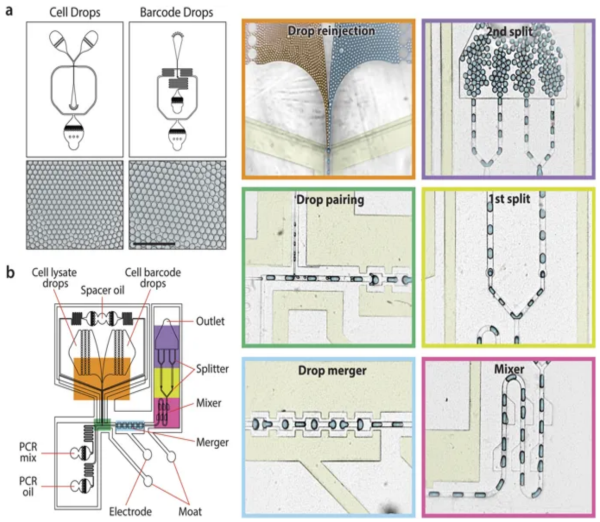

Fig. 6. Abseq droplet generation device summary (Shahi, P., Kim, S., Haliburton, J. et al. 2017)

III. Detailed fabrication

Procedures

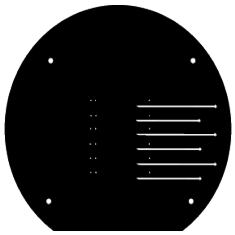

Fig. 7. Base Layer Mask

1) Base Layer: Since there is no valve actuation in the base layer, we choose to fabricate channels with rectangular cross-sections. Thus, we choose to use a negative photoresist, SU-8, to create the channel mold. We take a cleaned silicon wafer (cleaned by reactive ion etching followed by DI water wash) and spin coat SU-8 50 and spin coat at 2000rpm for 1 min. This gives us a height of about $50\,\mu\mathrm{m}$[**?**]. We pre-bake at 65°C for 6 minutes and softbake at 95°C for 20 minutes. We expose with about $300\,\mathrm{mJcm}^{-2}$ energy through the mask. We develop for about 6 minutes. We rinse with isopropyl alcohol and dry with nitrogen gas. hard bake is not required per the SU-8 datasheet [**?**]. To facilitate release, we expose to trimethylchlorosilane gas for 1 min. Once it is released, we transfer to a plastic dish [**?**].

Next, we use General Electric Silicones RTV 615 elastomer for our PDMS slab. In order to achieve a thickness of approximatelty 100 $200\,\mu\mathrm{m}$, we will spin coat at 1000 rpm for 25 seconds, based on estimates from literature [**?**]. The slab is baked at 80°C for 1.5 hours. To facilitate release, we expose to trimethylchlorosilane gas for 1 min. Once it is released, we transfer to a plastic dish. [**?**].

2) Micropillars: To fabricate micropillars, we follow the procedure outlined in literature. [**?**].

We then pour PDMS onto micropillars and follow the PDMS fabrication protocols outlined above.

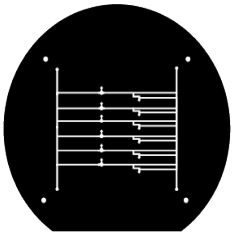

Fig. 8. Culture Layer Mask

3) Culture Layer: Because pneumatic control necessitates rounded parabolic channels, we choose to use positive photoresist AZ 100 XT PLP. to create channel molds [**?**], [**?**]. The protocol is almost identical to that of SU-8 (2000rpm for 1 min for a $50\,\mu\mathrm{m}$ height), save an additional step to create rounded cross-sections by heating to above the resin's glass-transition temperature (140°C for 5 min)[**?**].

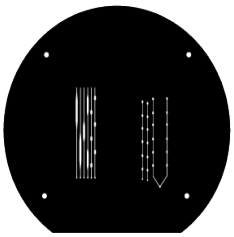

Fig. 9. Valve Layer Mask

4) Valve Layer: The photoresist mold for the channels is identical to that described for the base layer (with $50\,\mu\mathrm{m}$ height).

The PDMS slab is almost identical to the base layer as well, with the exception that because this is the top-most layer, we will cast it thick (2-3 mm) for mechanical stability and good interfacing with fluid pipes. Spin coating at this thickness is not needed [**?**].

5) Multilayer bonding: To enable bonding of all 4 of our device layers, we adopt multilayer soft lithography methods. GE RTV615 is a 2-component material containing polydimethylsiloxane bearing vinyl groups with a Pt catalyst and a Silicon Hydride cross-linker that binds vinyl groups. This is usually used in a 10:1 ratio. To enable binding, alternating layers may be made with 30:1 and 3:1 elastomers.

Separate slabs are cured by aligning and baking for 3 hours at 80°C. Care must be taken to drill access holes for the top layers before binding to bottom layers.

Scaling Considerations

Our device presents multiple avenues for which scaling may be of relevance. The scaling properties as a function of feature size were briefly discussed in our analysis of nutrient transport for chip 1. Throughput may be scaled up using multiple parallel channels for simultaneous experiments (addressed in conclusions) and actuation will require only $2 \cdot nlog_2 n + 3$ channels for n parallel experiments owing to the multiplexer design, which allows for individual channel control with relatively few pneumatic control valve channels and thus fewer fluid inlets. However, the distance between media channels

and the tumor culture well is contingent upon the number of multiplexer valves, so scaling may require greater migration channel widths which would, in turn, affect actuation pressures and/or actuation channel widths non-linearly; the actuation width and pressure was discussed in detail previously.

CONCLUSIONS

Cancer-associated fibroblasts (CAFs) are elusive players in cancer metasis. Normal fibroblasts are connective tissue cells that excrete ECM proteins. CAFs, however, secrete cytokines and proteins that cause ECM remodeling promoting tumor growth and extravasation. They may also play a role in angiogenesis and vasculogenesis. Furthermore, CAFs are unable to undergo apoptosis, indicating the involvement of various oncogenes or cancer associated cellular signaling [**?**]. The CAF-tumor interaction is not currently well-characterized, but its prevention is a promising pharmaceutical target.

It is also noteworthy that CAFs are not necessarily derived from fibroblasts, but can be induced from pericytes, epithelial cells, mesenchymal stem cells, bone marrow stromal cells, (CAF-candidates) and so on; CAF is thus more accurately a state as opposed to a cell type. There is thus no known deterministic protein marker unique to CAFs, although various combinations of markers are typically used to identify these cells [**?**].

Our device enables a better understanding of the transcriptomic profile of CAFs, which may be influenced by factors such as original cell type and tumor cell line. We can also use time as a parameter to understand how prolonged tumor-CAF interactions influence gene expression leading to phenotypic changes.

Proteins of interest may include apoptotic regulators (Bim/Bax/Bcl, caspases, etc.), growth factors (VEGF, TGF-β), tumorigenic proteins (such as Heat Shock Protein HSP1). Meta-analysis may further reveal novel markers corresponding to specific CAFs.

BIBLIOGRAPHY